

NANO EXPRESS

Open Access



Synthesis and Properties of Water-Soluble Blue-Emitting Mn-Alloyed CdTe Quantum Dots

Olena Tynkevych^{1*}, Volodymyr Karavan², Igor Vorona³, Svitlana Filonenko^{4,5} and Yuriy Khalavka¹

Abstract

In this work, we prepared CdTe quantum dots, and series of Cd_{1-x}Mn_xTe-alloyed quantum dots with narrow size distribution by an ion-exchange reaction in water solution. We found that the photoluminescence peaks are shifted to higher energies with the increasing Mn²⁺ content. So far, this is the first report of blue-emitting CdTe-based quantum dots. By means of cyclic voltammetry, we detected features of electrochemical activity of manganese energy levels formed inside the Cd_{1-x}Mn_xTe-alloyed quantum dot band gap. This allowed us to estimate their energy position. We also demonstrate paramagnetic behavior for Cd_{1-x}Mn_xTe-alloyed quantum dots which confirmed the successful ion-exchange reaction.

Keywords: Quantum dots, Cadmium telluride, Manganese, Alloying, Thioglycolic acid

Background

The optical properties of quantum dots (QDs) can be manipulated by doping/alloying through designing the composition. Consequently, the possibility of control over the incorporation of doping/alloying elements into QDs lattices plays an important role for a large number of applications. In particular, Mn-alloyed QDs are one of the most promising materials for fluorescence sensing and magnetic resonance imaging. Consequently, synthesis techniques have already been developed for obtaining Mn²⁺-doped/alloyed ZnS, ZnSe, CdSe, CdS, and core/shell CdTe/CdS QDs [1–6]. There is also a number of works that describe the capabilities of Mn²⁺- and Zn²⁺-doped/alloyed CdTe QDs synthesis [7–10]. Obtaining of such compositions in water solution is strongly pH-dependent that makes doping difficult. Cheng et al. showed that alkaline medium hindered the nucleation and growth of Zn-alloyed CdTe QDs [10]. Additionally, there is a high probability of appearance of Zn(OH)₂ on the surface of QDs that inhibits the growth of initial QDs by forming ZnO shell on the surface of QDs. Similar processes

take place in an attempt to prepare a Mn-alloyed CdSe QDs in alkaline aqueous solution [11]. In this case, Mn²⁺ solvation occurs instead of the ion exchange of Cd²⁺ by Mn²⁺. On the other hand, the difference of MnTe and CdTe solubility constant indicates ineffective substitution reaction between Mn²⁺ and CdTe [12].

In this work, we apply the synthetic procedure described in our previous work [13] for the synthesis of Cd_{1-x}Mn_xTe-alloyed QDs. To ensure a successful Mn-alloying process, the optimum neutral pH conditions were chosen. Such approach eliminated the formation of manganese hydroxide during the synthesis that allowed us to obtain blue-emitting Cd_{1-x}Mn_xTe-alloyed QDs by an ion-exchange reaction. The systematic studies of their optical and electrochemical properties enable a better understanding of the changes in the band structure during the transformation of CdTe QDs into Cd_{1-x}Mn_xTe-alloyed QDs.

Methods

Synthesis of CdTe and Cd_{1-x}Mn_xTe-alloyed QDs

Water-soluble thioglycolic acid-stabilized CdTe and Cd_{1-x}Mn_xTe-alloyed QDs were synthesized according to our previously reported modified three-step method [13]. Firstly, CdTe nanoclusters were synthesized using a facile room temperature method [14] with thioglycolic

* Correspondence: o.tynkevych@chnu.edu.ua

¹Yuriy Fedkovych Chernivtsi National University, Kotsiubynsky Str. 2, Chernivtsi 58012, Ukraine

Full list of author information is available at the end of the article

acid as a stabilizer. The obtained CdTe nanoclusters were divided into six different 50 ml aliquots. Secondly, obtained colloidal solutions of CdTe nanoclusters were subjected to Mn^{2+} alloying due to ion exchange process with different amounts of MnSO_4 salt in 50 ml aliquots solutions under sonication. The concentrations of Mn^{2+} ions added were 1, 5, 10, 15, and 20% of Cd^{2+} content in the reaction mixtures (RM). Also, one aliquot of pure CdTe nanoclusters was used as a control. The final step was a thermal treatment possess by microwave heating in the microwave oven at 700 W for 3 min.

Material Characterization and Measurement Procedures

Absorption and photoluminescence (PL) spectra were measured at room temperature by the OceanOptics USB-2000 spectrophotometer. The cyclic voltammograms (CV) were recorded using a computer-controlled Potentiostat/Galvanostat "ПИ-50-1." A three-electrode system consisted of a platinum working electrode, a glassy carbon counter electrode, and an Ag/AgCl reference electrode was used. The cyclic voltammograms were obtained by scanning the potential from -2 to 2 V at a scan rate of 100 mV s^{-1} . Transmission electron microscopy (TEM) images obtained with Selmi TEM-125 K microscope at an accelerating voltage of 80.00 kV. The elemental analysis of water-soluble $\text{Cd}_{1-x}\text{Mn}_x\text{Te}$ -alloyed QD samples purified by multiple precipitations was measured by C115M1 atomic emission spectroscopy (AES). EPR spectra were recorded using X-band EPR spectrometer "Radiopan" at 300 K. One hundred kilohertz modulation of the magnetic field with 0.1 mT amplitude. Visual EPR programs were used for the processing (deconvolution, fitting, and modeling) of the spectra obtained [15]. Powder samples containing QDs

were prepared by precipitation of QDs from the aqueous solution by the method described in [16]. The samples were dried at 35°C for 5 h. Phase composition of the samples was determined by powder XRD measurements using Bruker D8 Advance diffractometer. The identification of the crystalline phase of $\text{Cd}_{1-x}\text{Mn}_x\text{Te}$ was made using the XRD database card: ICSD no. 040413 (Match! software version 3.6.0.111).

Results and Discussion

Structural Characterization of the CdTe and $\text{Cd}_{1-x}\text{Mn}_x\text{Te}$ -alloyed QDs

TEM Analysis

The TEM images of $\text{Cd}_{0.91}\text{Mn}_{0.09}\text{Te}$ -alloyed QDs indicated that the average diameter is consistent with the diameter of CdTe QDs calculated from the spectroscopic measurements according to the method described in [14]. Figure 1 shows a TEM image for $\text{Cd}_{0.91}\text{Mn}_{0.09}\text{Te}$ -alloyed QDs. The vast majority of QDs with an average size of $2.3 \pm 0.3 \text{ nm}$ were observed. This confirms our assumption that the particles' size remains unchanged during Mn alloying. Also, larger irregularly shaped objects were observed. It can be seen that those objects are consist of multiple QDs of smaller diameter. Based on these data, we can conclude that bigger objects are aggregates formed during the preparation of the samples for TEM analysis.

Atomic Emission Spectroscopy Analysis

It was previously shown that only about 20% of the Cd^{2+} ions of the precursor solution participate in the formation of the CdTe QDs by this method of synthesis [13].

The elemental composition of the CdTe and the series of $\text{Cd}_{1-x}\text{Mn}_x\text{Te}$ -alloyed QDs were determined by atomic

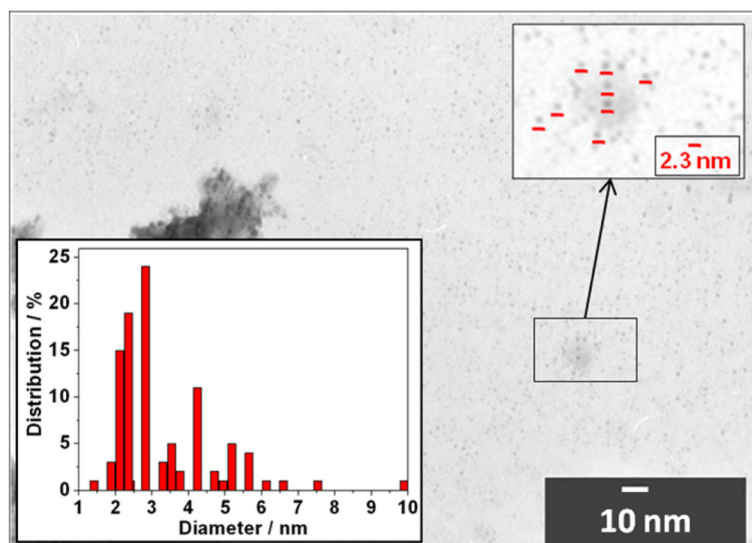


Fig. 1 TEM image of $\text{Cd}_{0.91}\text{Mn}_{0.09}\text{Te}$ -alloyed QDs. Inset: histogram illustrating the $\text{Cd}_{0.91}\text{Mn}_{0.09}\text{Te}$ -alloyed QD diameter distribution

emission spectroscopy (AES). Cadmium and manganese content was evaluated by the ratio of Cd:Mn (mg/l) for series of Cd_{1-x}Mn_xTe-alloyed QDs with different content of Mn²⁺ ions (Table 1).

It is interesting to note that Mn alloying has occurred unevenly with the increasing Mn²⁺ concentration in the reaction mixtures. It is clearly seen that addition at about 1% Mn²⁺ ions (relative to the content of Cd²⁺ ions in the reaction mixture) to the freshly prepared colloidal solution of CdTe nanoclusters leads to the formation of Cd_{0.96}Mn_{0.04}Te-alloyed QDs. On the other hand when the concentration of added Mn²⁺ was 5%, the formation of Cd_{0.97}Mn_{0.03}Te-alloyed QDs was observed. This disagreement may suggest that Mn-alloying process is more efficient in the presence of a minor excess of the alloying component. A further addition of 10, 15, and 20% Mn²⁺ ions leads to a consistent Mn alloying with CdTe QDs.

Spectroscopic Characterization

The optical properties of the prepared CdTe and Cd_{1-x}Mn_xTe-alloyed QDs were studied by means of Vis region absorption and fluorescence spectra. Figure 2 illustrates a typical absorption (a) and PL spectra (b) of CdTe and series of Cd_{1-x}Mn_xTe-alloyed QDs. Depending on the incorporated Mn²⁺ into CdTe, we observed a hypsochromic shift of the absorption peaks to the shorter wavelength. Also, the blue shift of the PL peaks from 542 to 496 nm was observed. There is a certain mismatch of hypsochromic shift of absorption and PL peaks for the samples 2 (red line) and 3 (blue line) which is probably caused by irregular Mn alloying.

It should be noted that the fluorescence intensity of the Cd_{1-x}Mn_xTe-alloyed QDs decreased with increasing of Mn²⁺ ion content (Additional file 1: Figure S1). It can be explained by the partial conjunction of Mn²⁺ ions that do not participate in alloying process and presence of a stabilizer (thioglycolic acid), which can quench QDs fluorescence [17].

Cyclic Voltammetric Characterization

A cyclic voltammetry (CV) method was applied to understand band structure changes as the result of the transformation of CdTe QDs into Cd_{1-x}Mn_xTe-alloyed QDs due to the increasing of Mn²⁺ content.

On typical CV of colloidal CdTe QDs, we observed (Fig. 3a) cathodic and anodic peaks at -1.00 V (marked as C1) and 1.48 V (marked as A1), respectively. The bandgap energy value of 2.48 eV, calculated according to the method described in [18], agrees well with the optical band gap of 2.50 eV obtained from the absorption peak maxima.

Basing on the optical properties of Cd_{1-x}Mn_xTe-alloyed QDs, we expected to observe oxidation at more positive potentials and reduction at more negative potentials for Cd_{1-x}Mn_xTe-alloyed QDs, with increasing of Mn²⁺ content in Cd_{1-x}Mn_xTe-alloyed QDs due to increasing of band gap energy. However, the separation between oxidation peak A2 and reduction peak C2 is too small to correlate with the band gap energy calculated from photoluminescence spectra. Interestingly, the potential difference of 2.18 V between C2 and A2 is absolutely identical for the whole series of Cd_{1-x}Mn_xTe-alloyed QDs samples (Fig. 3a, b).

As shown by Beaulac et al., excitonic PL decay times as long as 5 μs were observed for colloidal Cd_{1-x}Mn_xSe ($x = 0.004 \pm 0.002$) QDs ($d \approx 2.2$ nm) at 293 K, which arise as a result of thermal equilibrium between the CdSe excitonic states and the very long-lived ligand-field excited state of the Mn²⁺ dopants. Therefore, Mn doping does not quench the excitonic PL of Cd_{1-x}Mn_xSe QDs. Instead, itself-quenching effects of Mn²⁺ PL by thermally assisted back-energy transfer to the Cd_{1-x}Mn_xSe QDs excitonic states take place. [4].

We can assume that in the case of colloidal Cd_{1-x}Mn_xTe-alloyed QDs ($d \approx 2.3$ nm) at room temperature, a very similar phenomenon occurs. Using the CV method, the electrochemical activity of “dark” manganese energy levels inside the Cd_{1-x}Mn_xTe-alloyed QDs band gap was detected (Fig. 3b, c). Optical properties of Cd_{1-x}Mn_xTe-alloyed QDs show an increase of the band gap energy with increase of Mn²⁺ content as result of back-energy transfer phenomena (Fig. 3d).

XRD Analysis

Additional file 1: Figure S2 shows the XRD spectra for CdTe and series of Cd_{1-x}Mn_xTe-alloyed QD dried samples which were precipitated from an aqueous solution using isopropyl alcohol.

Table 1 The Cd²⁺/Mn²⁺ ratio in the reaction mixtures (RM) and in the QDs as determined by AES measurements

Sample ID	QDs composition	Ratio Cd ²⁺ /Mn ²⁺ (RM)	Ratio Cd ²⁺ /Mn ²⁺ (QDs/RM)	Ratio Cd ²⁺ /Mn ²⁺ (QDs)
1	CdTe	1/0	0.20/0	1/0
2	Cd _{0.96} Mn _{0.04} Te	1/0.01	0.20/0.01	0.96/0.04
3	Cd _{0.97} Mn _{0.03} Te	1/0.05	0.20/0.05	0.97/0.03
4	Cd _{0.95} Mn _{0.05} Te	1/0.10	0.20/0.10	0.95/0.05
5	Cd _{0.92} Mn _{0.08} Te	1/0.15	0.20/0.15	0.92/0.08
6	Cd _{0.91} Mn _{0.09} Te	1/0.20	0.20/0.20	0.91/0.09

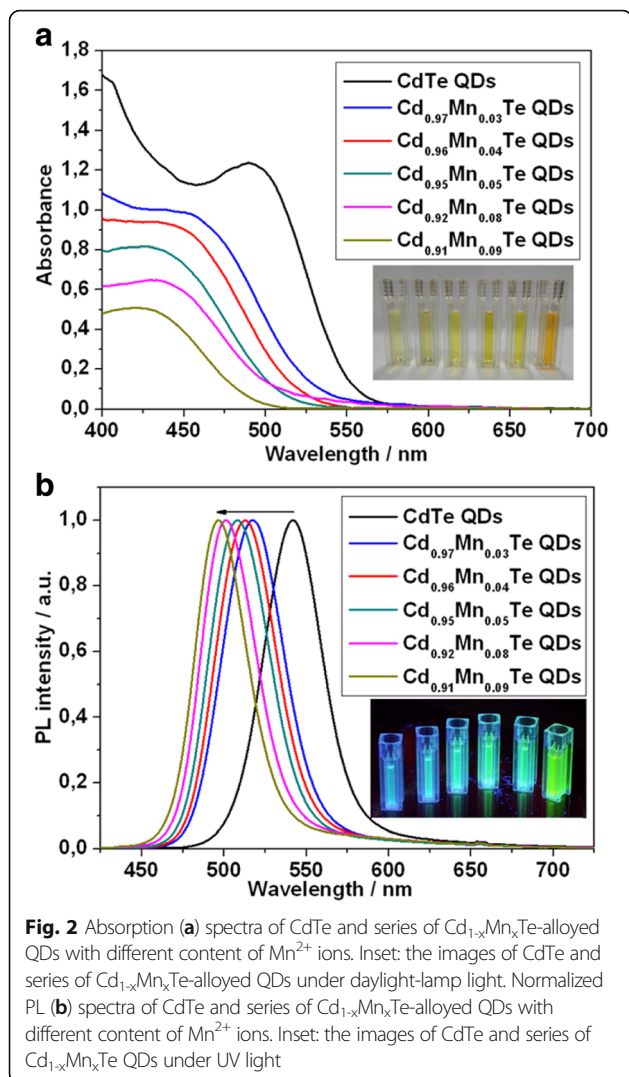


Fig. 2 Absorption (a) spectra of CdTe and series of $\text{Cd}_{1-x}\text{Mn}_x\text{Te}$ -alloyed QDs with different content of Mn^{2+} ions. Inset: the images of CdTe and series of $\text{Cd}_{1-x}\text{Mn}_x\text{Te}$ -alloyed QDs under daylight-lamp light. Normalized PL (b) spectra of CdTe and series of $\text{Cd}_{1-x}\text{Mn}_x\text{Te}$ -alloyed QDs with different content of Mn^{2+} ions. Inset: the images of CdTe and series of $\text{Cd}_{1-x}\text{Mn}_x\text{Te}$ QDs under UV light

The XRD spectrum for CdTe QDs scanning over the two theta range of 20° – 60° shows diffraction peak at 25° , which is assigned to the (111) crystal planes of CdTe with cubic crystalline structure [19]. This peak is significantly wider than that of the bulk materials due to the small size of QDs with narrow size distribution. The signal on XRD patterns of all series of $\text{Cd}_{1-x}\text{Mn}_x\text{Te}$ -alloyed QDs is shifted toward higher angles. The peak at 30° – 35° can be deconvoluted into two peaks at 30° and 35° , which are assigned to the (200) and (220) planes of $\text{Cd}_{1-x}\text{Mn}_x\text{Te}$ alloy. These results may indicate the formation of $\text{Cd}_{1-x}\text{Mn}_x\text{Te}$ with cubic structure. Such XRD data confirm that the CdTe QDs underwent the Mn-alloying process successfully. Notably that peak centered at 25° decays on XRD pattern of $\text{Cd}_{0.97}\text{Mn}_{0.03}\text{Te}$ alloyed QDs and vanishes on the XRD patterns of the samples with higher Mn^{2+} content. In the case of $\text{Cd}_{0.97}\text{Mn}_{0.03}\text{Te}$ QDs

sample, we concluded formation of core/shell CdTe/ $\text{Cd}_{1-x}\text{Mn}_x\text{Te}$ QDs where the signal of $\text{Cd}_{1-x}\text{Mn}_x\text{Te}$ shell screens the signal of CdTe core. For all subsequent samples, one broad diffraction peak at 30° – 35° can testify the further Mn alloying of CdTe QDs and formation of a thicker $\text{Cd}_{1-x}\text{Mn}_x\text{Te}$ shell. Generally, this leads to the formation of QDs with higher manganese contents.

EPR Measurements

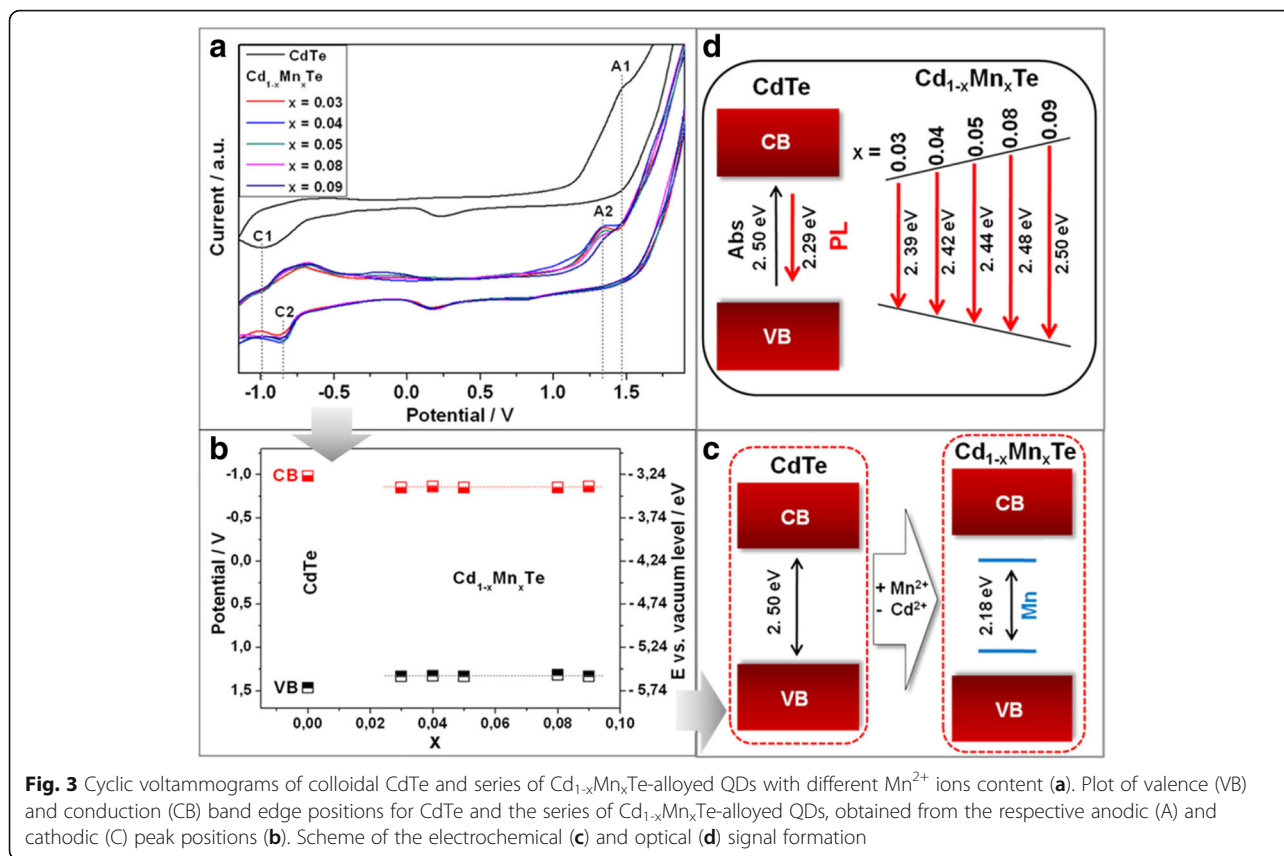
The EPR spectra of $\text{Cd}_{0.97}\text{Mn}_{0.03}\text{Te}$ -alloyed QDs are shown in Fig. 4. The spectrum consists of six asymmetric lines that are superimposed on the broad underlying signal. The presence of six lines in the spectrum is typical for Mn^{2+} ions in the disordered systems [2, 20–22]. However, the shape of the spectrum is more complex than the trivial Mn^{2+} -related signal. A detailed analysis has shown that experimental EPR spectrum can be described as a superposition of three signals: broad Gaussian with a linewidth of 50 mT and two sextets with lines spaced by 10 and 6 mT, respectively.

Gaussian-shape EPR signal centered at $g = 2.0069$ (signal 2) can be attributed to Mn^{2+} ions interconnected by dipole-dipole interaction. These ions are located in regions with a high local concentration of manganese and interact with each other. Due to the lines broadening a strong dipole-dipole interaction between manganese ions masks the specific spectral features being characteristic for isolated manganese ions and leads to a single-line EPR signal. The two other EPR signals (marked as 3 and 4) should be assigned to isolated Mn^{2+} ions. To determine the parameters of isolated Mn^{2+} ions and its location the spin-Hamiltonian containing electronic, nuclear Zeeman interaction, hyperfine interaction, and the interaction of the electron spin with the crystal field (zero-field splitting term) was used:

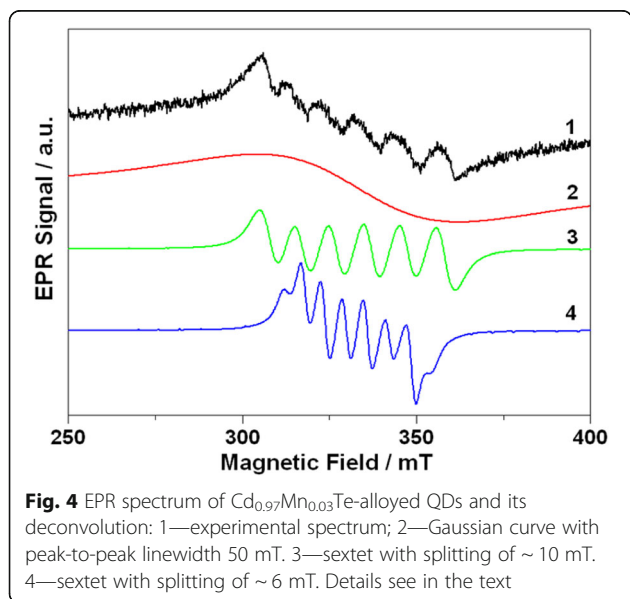
$$\hat{H} = g\beta\mathbf{B}\mathbf{S} - g_N\beta_N\mathbf{B}\mathbf{I} + \mathbf{A}\mathbf{S}\mathbf{I} + \sum_{n,m} b_n^m O_n^m$$

where β and β_N denote the Bohr and nuclear magnetons, respectively; \mathbf{B} is the external magnetic field; g and g_N are the electron and nuclear g -tensors, respectively; \mathbf{A} is the tensor of the hyperfine interaction; \mathbf{S} and \mathbf{I} are the electron and nuclear quantum-mechanical spin operators, respectively; and b_n^m and O_n^m are the crystal field constants and quantum-mechanical operators, respectively. The values of g , g_N , β , β_N , and A are assumed to be isotropic (that being characteristic for Mn^{2+} ions in II-VI compounds). The set of b_n^m parameters is determined by the surroundings of Mn^{2+} and depends on the symmetry of the ions positions.

The signal 2 can be described by the parameters $g = 2.0069$ and $A = -94.5 \times 10^{-4} \text{ cm}^{-4}$ that can be assigned to the isolated Mn^{2+} ions located in the position near



the surface of QDs. At the same time, signal 3 was found to be characterized by parameters $g = 2.0069$, $A = -57.5 \times 10^{-4} \text{ cm}^{-4}$ and $b_4^0 = 27.7 \times 10^{-4} \text{ cm}^{-4}$. This set of parameters is typical for Mn²⁺ in cation position (Mn_{Cd}) of bulk CdTe crystals.



Conclusions

The synthesis of blue-emitting Cd_{1-x}Mn_xTe-alloyed QDs of small size was developed. The systematic study of their optical and electrochemical properties has been provided. The blue shift of the PL peaks from 542 to 496 nm during the increasing the Mn²⁺ content in Cd_{1-x}Mn_xTe-alloyed QDs was observed. XRD and EPR analysis confirm the successful replacement of cadmium by manganese ions in the process of synthesis. Colloidal Cd_{1-x}Mn_xTe-alloyed QDs show an increase of the band gap energy with increasing Mn²⁺ content at room temperature as a result of thermally assisted back-energy transfer.

Additional File

Additional file 1: Figure S1. The Mn²⁺ content dependence of the photoluminescence integral intensity and the photoluminescence energy maximum of the CdTe QDs and series of Cd_{1-x}Mn_xTe-alloyed QDs. **Figure S2.** XRD patterns for CdTe QDs and series of Cd_{1-x}Mn_xTe-alloyed QDs. (DOCX 153 kb)

Abbreviations

CV: Cyclic voltammetry; EPR: Electron paramagnetic resonance; PL: Photoluminescence; QDs: Quantum dots; TEM: Transmission electron microscopy; TGA: Thioglycolic acid; XRD: X-ray diffraction

Acknowledgements

We are grateful to Dr. Oleksandra Korovianko and MSc Olena Khamkevych for the assistance in the QD preparation and discussion of the obtained results.

Funding

This work was partially supported by the Ministry of Education and Science of Ukraine (Grants:#0116U001447 "Optically active materials based on metallic and semiconductor nanocrystals embedded into the crystalline and amorphous matrix" and #0116U006958 "Multifunctional nitrogen-containing heterocyclic antioxidants as effective retarders of process photodegradation of quantum dots in optically active materials").

Authors' Contributions

OT performed the synthesis of CdTe and Cd_{1-x}Mn_xTe-alloyed QDs, performed the CV and optical measurements with related calculations, prepared the samples for other methods of analysis, analyzed and discussed the obtained data, and wrote the manuscript. VK performed the AES analysis and discussed the obtained results. IV has provided EPR measurements with related calculations and assisted in manuscript writing. SF performed the XRD measurement and the analysis of received data and contributed to the result discussion. YK has contributed to the result discussion and main conclusion suggestion and assisted in manuscript writing. All authors read and approved the final text of the manuscript.

Competing Interests

The authors declare that they have no competing interests.

Publisher's Note

Springer Nature remains neutral with regard to jurisdictional claims in published maps and institutional affiliations.

Author details

¹Yuriy Fedkovych Chernivtsi National University, Kotsiubynsky Str. 2, Chernivtsi 58012, Ukraine. ²The Scientific Center of Preventive Toxicology, Food and Chemical Safety, Fedkovycha Str. 30, Chernivtsi 58000, Ukraine. ³V. Lashkaryov Institute of Semiconductor Physics of National Academy of Sciences of Ukraine, 45, Pr. Nauky, Kyiv 03028, Ukraine. ⁴L. V. Pisarzhevskii Institute of Physical Chemistry of National Academy of Sciences of Ukraine, 31, Pr. Nauky, Kyiv 03028, Ukraine. ⁵Aalto University School of Science, P.O. Box 12200, FI-00076 Aalto, Finland.

Received: 29 December 2017 Accepted: 16 April 2018

Published online: 02 May 2018

References

- Zhuang J, Zhang X, Wang G, Li D, Yang W, Li T (2003) Synthesis of water-soluble ZnS:Mn²⁺ nanocrystals by using mercaptopropionic acid as stabilizer. *J Mater Chem* 13:1853–1857
- Nosenko V, Vorona I, Grachev V, Ishchenko S, Baran N, Yu B, Zhuk A, Yu P, Kladko V, Selishchev A (2016) The crystal structure of micro- and nanopowders of ZnS studied by EPR of Mn²⁺ and XRD. *Nanoscale Res Lett* 13:517–523
- More D, Rajesh C, Lad AD, Kumar GR, Mahamuni S (2010) Two photon absorption in Mn²⁺-doped ZnSe quantum dots. *Opt Commun* 283:2150–2154
- Beaulac R, Archer PI, van Rijssel J, Meijerink A, Gamelin DR (2008) Exciton storage by Mn²⁺ in colloidal Mn²⁺-doped CdSe quantum dots. *Nano Lett* 9: 2949–2953
- Sun D, Zhong H, Yao X, Chang Y, Zhao Y, Jiang Y (2014) A bright blue-shifted emission from Mn²⁺-doped CdS quantum dots. *Mater Lett* 125:132–135
- Li W, Sheng P, Feng H, Yin X, Zhu X, Yang X, Cai Q (2014) Stable core/shell CdTe/Mn-CdS quantum dots sensitized three-dimensional, macroporous ZnO nanosheet photoelectrode and their photoelectrochemical properties. *ACS Appl Mater Interf* 6:12353–12362
- Gao F, Li J, Wang F, Yang T, Zhao D (2015) Synthesis and characterization of high-quality water-soluble CdMnTe quantum dots capped by *N*-acetyl-L-cysteine through hydrothermal method. *J Lumin* 159:32–37
- Zhang F, He F, He XW, Li WY, Zhang YK (2014) Aqueous synthesis of highly luminescent surface Mn²⁺-doped CdTe quantum dots as a potential multimodal agent. *Luminescence* 29:1059–1065
- Zhao D, Fang Y, Wang H, He Z (2011) Synthesis and characterization of high-quality water-soluble CdTe:Zn²⁺ quantum dots capped by *N*-acetyl-L-cysteine via hydrothermal method. *J Mater Chem* 21:13365–13370
- Cheng J, Li D, Cheng T, Ren B, Wang G, Li J (2014) Aqueous synthesis of high-fluorescence CdZnTe alloyed quantum dots. *J Alloy Compd* 589:539–544
- Blaskin VA, Barrows CJ, Erickson CS, Gamelin DR (2013) Nanocrystal diffusion doping. *J Am Chem Soc* 135:14380–14389
- Xu S, Wang C, Zhang H, Sun Q, Wang Z, Cui Y (2012) Discriminative detection of bivalent Mn ions by a pH-adjustable recognition method via quantum dot fluorescence sensing. *J Mater Chem* 22:9216–9221
- Tynkevych OO, Ranoszek-Soliwoda K, Grobelny J, Selishchev OV, Khalavka YB (2016) Spectroscopic and electrochemical monitoring of band structure changes during the alloying of CdTe QDs by Hg²⁺ ions. *Mater Res Express* 3:105046–105052
- Rogach AL, Franzl T, Klar TA, Feldmann J, Gaponik N, Lesnyak V, Shavel A, Eychmüller A, Rakovich YP, Donegan JF (2007) Aqueous synthesis of thiol-capped CdTe nanocrystals: state-of-the-art. *J Phys Chem C* 111:14628–14637
- Grachev VG. www.visual-epr.com.
- Chang Y, Yao X, Zhang Z, Jiang D, Yu Y, Mi L, Wang H, Li G, Yu D, Jiang Y (2016) Spectroscopic and electrochemical monitoring of band structure changes during the alloying of CdTe QDs by Hg²⁺ ions. *Mater Res Express* 3:105046–105052
- Lou Y, Zhao Y, Chen J, Zhu JJ (2014) Metal ions optical sensing by semiconductor quantum dots. *J Mater Chem C* 2(4):595–613
- Kucur E, Riegler J, Urban GA, Nann T (2003) Determination of quantum confinement in CdSe nanocrystals by cyclic voltammetry. *J Chem Phys* 119: 2333–2337
- Wang Y, Liu S (2012) One-pot synthesis of highly luminescent CdTe quantum dots using sodium tellurite as tellurium source in aqueous solution. *J Chilean Chem Soc* 57:1109–1112
- Counio G, Esnouf S, Gacoin T, Boilot JP (1996) CdS:Mn nanocrystals in transparent Xerogel matrices: synthesis and luminescence properties. *J Phys Chem* 100:20021–20026
- Jing L, Ding K, Kalytchuk S, Wang Y, Qiao R, Kershaw SV, Rogach AL, Gao M (2013) Aqueous manganese-doped core/shell CdTe/ZnS quantum dots with strong fluorescence and high relaxivity. *J Phys Chem C* 117:18752–18761
- Dantas NO, Fernandes GL, Baffa O, Gómez JA, Silva ACA (2015) Controlling densities of manganese ions and cadmium vacancies in Cd_{1-x}Mn_xTe ultrasmall quantum dots in a glass matrix: x-concentration and thermal annealing. *J Phys Chem C* 119(30):17416–17420

Submit your manuscript to a SpringerOpen journal and benefit from:

- Convenient online submission
- Rigorous peer review
- Open access: articles freely available online
- High visibility within the field
- Retaining the copyright to your article

Submit your next manuscript at ► springeropen.com